Journal of Rock Mechanics and Geotechnical Engineering 10 (2018) 678–693

Contents lists available at ScienceDirect

Journal of Rock Mechanics and Geotechnical Engineering

journal homepage: www.rockgeotech.org

Full Length Article

A laboratory study of stress arching around an inclusion due to pore pressure changes

Hani Asaei, Mahdi Moosavi*, Mohammad Ali Aghighi

University of Tehran, Tehran, Iran

ARTICLE INFO

Article history:
Received 7 August 2017
Received in revised form
29 January 2018
Accepted 31 January 2018
Available online 31 May 2018

Keywords:
Stress arching
Laboratory test
Large-scale sample
Synthetic sandstone

ABSTRACT

When the pore pressure in a porous rock changes, stress arching will occur within the rock and the surrounding region. Stress arching ratio is defined as the total stress changes in the porous rock to the pore pressure change in the region. The region may have the same or different elastic moduli with the surrounding rock, which is usually referred to as inclusion or inhomogeneity. Stress arching is responsible for many geomechanical problems encountered during production or injection; in addition, it is a crucial parameter in stress estimation during field development. This paper aims to present laboratory measurements of vertical stress arching ratio in a material surrounding the inclusion (inhomogeneity). To the authors' knowledge, few laboratory experiments have been reported on direct measurement of stress arching. The inclusion is a cylindrical sandstone (44 mm in diameter and 50 mm in height) embedded in a larger cylindrical sandstone (150 mm in diameter and 154 mm in height), both of which are made synthetically. These two parts are separated and sealed by a internal polyurethane sleeve. Vertical stress changes are recorded by a mini hydraulic sensor embedded in surrounding rock. Laboratory results are compared to those obtained by numerical models. These models are checked with analytical formulations. The results of numerical models show a good agreement with laboratory data. The numerical results also indicate that the sensor response is affected by elastic properties of the internal sleeve. According to the sensitivity analysis performed, in the absence of the internal sleeve, properties of the inclusion have significant effects on the surrounding stress arching induced.

1. Introduction

Pore pressure changes in a porous medium promote changes in stresses due to effective stress law and stress arching. The effective stress law introduced by Terzaghi (1925) and Biot (1941) indicate that stress in rock skeleton is determined by subtracting a percentage of pore pressure from total stress, while the total stress remains unchanged. Stress arching causes change in the total stress within and around a reservoir. Repeated stress measurements in a number of oil fields have revealed that there is a reduction in the total minimum horizontal stress during reservoir depletion, as shown in Fig. 1 schematically. According to Fig. 1, depletion of reservoir causes decrease in reservoir's total horizontal stress in addition to reservoir pressure. The total stress change that accompanies the reservoir pressure change is known as the "stress arching". When the stress arching is generated due to reservoir depletion, partial amount of total stress is supported by the surrounding formations. The total stress changes induced by fluid production or injection (stress arching) can have negative consequences such as cap rock failure, fault reactivation, and wellbore and casing damage (Hillis, 2003; Sayers, 2006; Soltanzadeh et al., 2007; Wang et al., 2015).

Ignoring stress arching can cause considerable errors in engineering design, as shown in Fig. 2. In Mohr circle representation of stresses, when the pore pressure changes with constant total stress (no stress arching), a shift in Mohr circle location is induced without diameter change (Fig. 2a). When the stress arching is considered, the diameter of Mohr circle changes due to pore pressure changes. In other words, the stress arching of total stresses causes development of deviatoric stresses and change of Mohr circle diameter (Fig. 2b). This fact is the reason for unexpected rock behavior in depletion or injection scenarios (Segura et al., 2011; Lynch et al., 2013).

* Corresponding author.
E-mail addresses: haniasaei@ut.ac.ir (H. Asaei), mmoosavi@ut.ac.ir (M. Moosavi), m.aghighi@ut.ac.ir (M.A. Aghighi).

Peer review under responsibility of Institute of Rock and Soil Mechanics, Chinese Academy of Sciences.

https://doi.org/10.1016/j.jrmge.2018.01.008

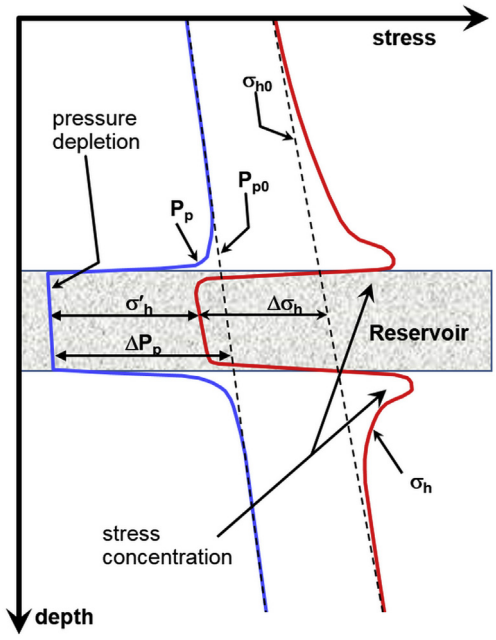

Fig. 1. Horizontal stress arching within and around a reservoir. Dashed lines are the initial stress and reservoir pressure profiles before depletion. Solid lines denote the horizontal stress and reservoir pressure profiles after depletion.

Generally, stress arching in porous media occurs within and around a region that has different conditions from surrounding materials (such as differences in pore pressure, temperature and mechanical properties). In this paper, the effects of pore pressure change in the region and the mechanical properties of materials within and around the region are discussed. According to Eshelby's theories of inclusion and inhomogeneity, when the elastic moduli of materials within and around the region are the same, it is called "inclusion", otherwise, it is referred to as "inhomogeneity" (Eshelby, 1957, 1959; Rudnicki, 1999, 2011; Soltanzadeh and Hawkes, 2007; Mura, 2013). The same definitions are used in this paper. However, the "inclusion" is used as a general term unless "inhomogeneity" is specifically discussed.

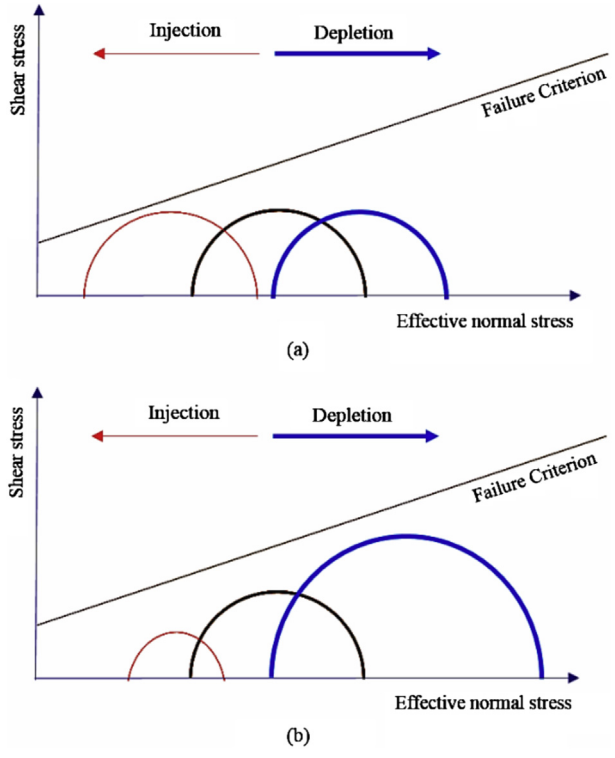

Fig. 2. Significance of stress arching in porous rock behavior. Blue circles represent the initial stress conditions. (a) In the case of ignoring stress arching, the diameters of Mohr circles are constant in reservoir injection or depletion; and (b) In the case of considering stress arching, the diameters of Mohr circles change due to injection or depletion.

Stress arching, also referred to as reservoir stress path (Goulty, 2003; Segura et al., 2011; Lynch et al., 2013), pore pressure-stress coupling (Hillis, 2003; Tingay et al., 2003; Altmann et al., 2014), or depletion/injection induced stress changes (Segall, 1992; Holt et al., 2004), is the ratio of total stress changes to the pore pressure change. According to Hettema et al. (2000), stress arching ratios are defined as follows:

$$\gamma_H = \frac{\Delta\sigma_H}{\Delta p_p}, \gamma_h = \frac{\Delta\sigma_h}{\Delta p_p}, \gamma_v = \frac{\Delta\sigma_v}{\Delta p_p} \tag{1}$$

where γ_H and γ_h are the horizontal stress arching ratios (in two perpendicular directions); γ_v is the vertical stress arching ratio; $\Delta\sigma_H$, $\Delta\sigma_h$, and $\Delta\sigma_v$ are the corresponding horizontal and vertical stress changes, respectively; and ΔP_p is the reservoir or inclusion pore pressure change. In the literature, deviatoric stress path (K) is defined as the ratio of horizontal effective stress change to the vertical effective stress change during pore pressure drawdown (Teufel et al., 1991; Khan and Teufel, 2000; Segura et al., 2011):

$$K = \frac{\Delta\sigma'_h}{\Delta\sigma'_v} \tag{2}$$

where K is a representative parameter for stress anisotropy. The relationship between Eqs. (1) and (2) is presented as (Segura et al., 2011):

$$K = \frac{1-\gamma_h/\alpha}{1-\gamma_v/\alpha} = \frac{\alpha-\gamma_h}{\alpha-\gamma_v} \tag{3}$$

where α is the Biot coefficient. According to the theory of poroelastisity, with assumptions of uniaxial strain boundary condition and no vertical stress arching, the horizontal stress arching is defined as follows (Segura et al., 2011):

$$\gamma_h = \frac{1-2\nu}{1-\nu} \tag{4}$$

where ν is the Poisson's ratio of rock. Eq. (4) is valid in ideal condition such as deep laterally extended reservoirs without natural complexity. In these reservoirs, the uniaxial strain boundary condition can be assumed with minimum error (Settari, 2002). In addition, overburden weight is fully transferred to the reservoirs without vertical stress arching because of their great width and small thickness (Goulty, 2003). It is clear that this assumption is not valid for many natural reservoirs because they do not have such ideal conditions. This has been confirmed by field measurements, and analytical and numerical analyses (Addis, 1997; Segall and Fitzgerald, 1998; Gambolati et al., 1999; Ruistuen et al., 1999; Hettema et al., 2000, 2009; Zoback and Zinke, 2002; Alassi et al., 2006; Sayers and Schutjens, 2007; Schutjens and Kuvshinov, 2010).

Analytical solutions show that, for particular geometries in an infinite medium such as sphere, cylinder and infinite layer, the following relationship holds among poroelastic stress arching ratios (Fjar et al., 2008):

Table 1
Properties and mineral compositions of inclusion and inhomogeneity for three tests.

Properties						
Tests	Cement content (%)	Mean grain size (mm)	Compaction stress (MPa)	Young's modulus (MPa)	Poisson's ratio	Biot coefficient
Inclusion	35	0.21	3	700	0.29	0.85
Soft inhomogeneity	15	0.38	3	450	0.35	0.9
Stiff inhomogeneity	35	1.28	3	1500	0.2	0.85
Mineral composition (%)						
SiO_2	Al_2O_3	Fe_2O_3	CaO	MgO	Na_2O	K_2O
97.6%	0.48	0.12	0.13	0.08	0.63	0.14

Note: Properties of the surrounding rocks are identical to those of the inclusion for all the tests.

$$\gamma_v + \gamma_H + \gamma_h = \alpha \frac{2(1-2\nu)}{1-\nu} \tag{5}$$

Stress arching has been studied in the literature from different points of view. The minimum horizontal stress arching has been measured and reported using hydraulic fracturing tests (Addis, 1997; Khan and Teufel, 2000; Soltanzadeh and Hawkes, 2009a; Altmann et al., 2010; Segura et al., 2011). The results showed that stress arching is a time-dependent parameter and even variable in different regions of reservoirs. The reported values range from 0.24 to 0.84 (Soltanzadeh and Hawkes, 2009a). Hydraulic fracturing tests are the most reliable method for evaluation of stress arching induced by production or injection, however, they are expensive.

Analytical studies for stress arching are limited to theories introduced by Geertsma (1973) (theory of strain nuclei) and Eshelby (1957, 1959) (theory of inclusion and inhomogeneity). The theory of strain nuclei solves field equations in an elastic medium under point loading conditions, such as point forces, concentrated moments, and centers of dilatation (or compression). Eshelby theory evaluates stress inside and around inclusions with different geometries by applying eigenvalue strain to the inclusions using continuum elastic formulation. These analytical methods have been developed and applied in poroelastisity and reservoir geomechanics (Segall, 1985; Segall et al., 1994; Segall and Fitzgerald, 1998; Rudnicki, 1999, 2002; Soltanzadeh and Hawkes, 2007, 2008). All the models are based on simplified geometrical and fluid flow assumptions. The limitation of the analytical methods is infinite or semi-infinite surrounding medium. Therefore, they are not applicable to finite media except some models limited to very simple geometry (Li et al., 2006a, b).

Numerical analyses and models are developed and used for evaluation of production/injection induced stress changes in reservoirs and surrounding area. These studies are applied to geomechanical design of fields, such as fault reactivation (Soltanzadeh and Hawkes, 2008, 2009b; Orlic and Wassing, 2013; Altmann et al., 2014), in-fill drilling and wellbore stability (Addis et al., 2001; Rutqvist et al., 2012), production induced permeability reduction and compaction (Ruistuen et al., 1999; Khan and Teufel, 2000; Schutjens et al., 2008; Wang et al., 2015), hydraulic fracturing and stress reversal (Wright et al., 1995; Aghighi and Rahman, 2010), spatial- and time-dependent stress distribution (coupled model) (Rudnicki, 1986), hysteresis behavior of reservoir (Lynch et al., 2013; Holt et al., 2016), and gas injection (Orlic, 2009; Lynch et al., 2013; Kim and Hosseini, 2017). Simple numerical models show that stress arching is dependent on the elastic moduli of materials within and around the reservoir, Biot coefficient and model geometry (Khan and Teufel, 2000; Segura et al., 2011).

In this paper, surrounding vertical stress arching is measured directly by a miniature pressure cell (called "sensor" in this paper) in the laboratory. For the tests, large-scale cylindrical samples of 154 mm in height and 150 mm in diameter are used. The samples are made of sand particles and have two parts separated by an internal polyurethane sleeve. The inclusion and the surrounding parts are both constructed synthetically in a determined process. To study the effect of inclusion mechanical properties on the stress arching in the surrounding materials, three main tests including inclusion test, soft inhomogeneity and stiff inhomogeneity tests are performed on the samples. Vertical stress arching is determined from the slope of the obtained curves. The results show that the surrounding vertical stress arching ratios obtained from inclusion test, soft inhomogeneity and stiff inhomogeneity tests are 0.13, 0.14 and 0.1, respectively.

Furthermore, laboratory test results are checked by numerical models. Numerical results show that the presence of internal sleeve with mechanical properties different from those of the porous rock decreases the stress arching ratio by approximately 100%. This suggests that the mechanical properties of intermediate layers between the reservoir and the surrounding materials have significant effects on the surrounding stress arching. The linear part of the curves, which represents the compressive stresses transferred through the surrounding materials during stress arching, is of interest in comparison to the nonlinear parts which constitute tensional and transitional stresses in the materials. The linear parts obtained from the laboratory tests and numerical models are in good agreement with each other. Sensitivity analysis of poroelastic coefficients shows that inclusion (inhomogeneity) properties have more effects on the vertical stress arching in the surrounding materials than those of the surrounding material itself.

2. Laboratory measurement of stress arching

This section explains the experimental methods used in this study to measure stress changes induced by depletion/injection. Experimental tests are carried out on the large-scale synthetic sandstone samples with two separated parts under conditions that the mechanical properties of the internal region are either identical to (inclusion test) or different from those of the surrounding rock (inhomogeneity test). In the following sections, synthetic sandstone production procedure, laboratory system, sensor calibration test and main test procedures are explained briefly.

2.1. Synthetic sample production

The samples are 154 mm in height and 150 mm in diameter with a cylindrical inclusion at the top and inside the surrounding part. The inclusion with the height of 50 mm and diameter of 40 mm is separated by an internal polyurethane sleeve of 2 mm thick to enable independent pore pressure change from the surrounding part. Three synthetic samples are made for one inclusion test and two inhomogeneity tests. Properties of the synthetic samples and their mineral compositions are shown in Table 1. The properties of the surrounding material for all samples are identical to those of the inclusion, as listed in Table 1. Note that many NX-size samples

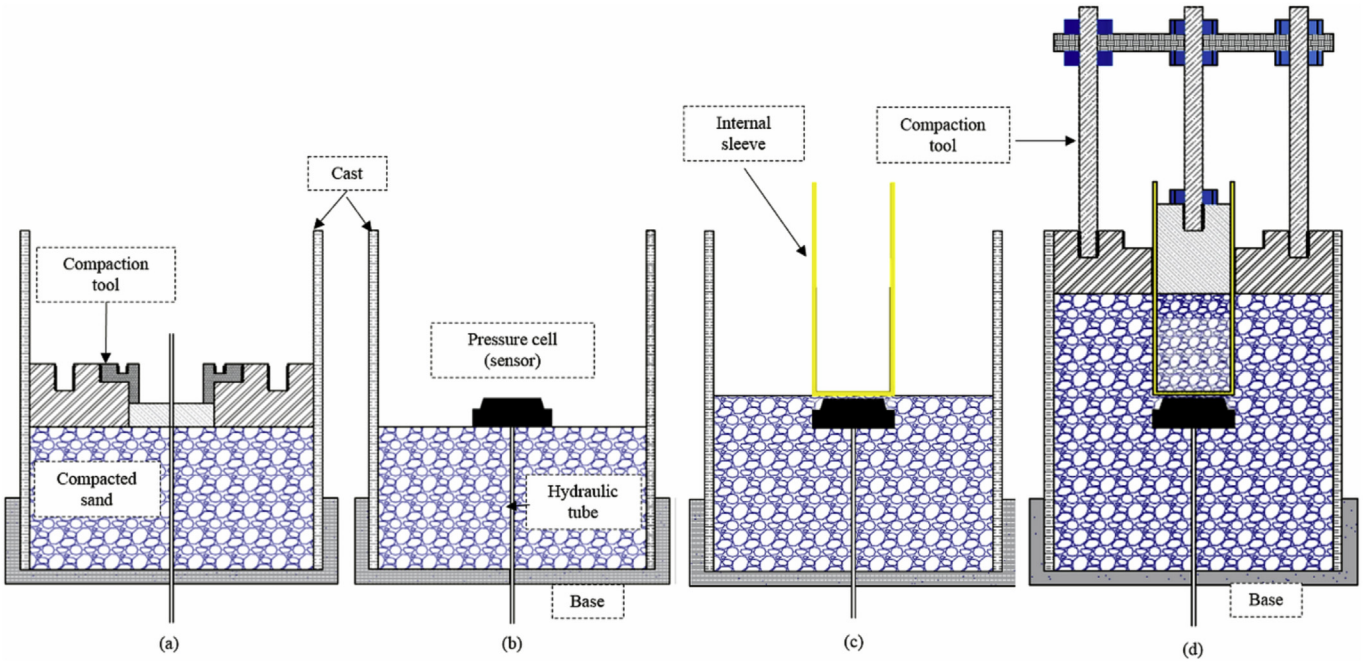

Fig. 3. Production procedures of synthetic sample: (a) Sand mixture is compacted until the sensor is placed using the compaction tool; (b) The sensor is placed in the surrounding material; (c) After the sensor's embedment, the internal sleeve is placed above the sensor at the distance of 2 mm; and (d) The inclusion and the surrounding material are compacted using the compaction tool simultaneously.

are made synthetically and are tested to choose intended material properties for main tests.

Synthetic samples are prepared using the procedures described in Asaei and Moosavi (2013). A mixture of sand, cement and water undergoes a staged compaction in a cylindrical cast until the cast is full. In Fig. 3, a schematic view of synthetic sample production is shown in four stages. At first, the mixture is compacted until a sensor is placed using a compaction tool. Then the sensor is moved to the center and the sand mixture is fully compacted. The thickness of the compacted sand above the sensor is 2 mm. After the sensor is embedded in the surrounding material, the internal sleeve is placed at the center. At the final stage, the inclusion and the surrounding material are compacted using the compaction tool. As shown in Fig. 4, the compaction tool is designed to compact the inclusion and the surrounding sand simultaneously; in addition, it helps to centralize the sensor and the internal sleeve during sample production. Fig. 5 presents some stages of sample production in the laboratory. It is noted that compaction tests for different sand mixtures are performed to determine the volume of poured sand mixture in the cast at each stage of sample production. After filling the cast, it is kept in the ambient condition for 24 h. Then, it is put in an air bath inside water at 80 °C for 24 h for cement curing. Subsequently, the sample is separated from the cast and dried in an

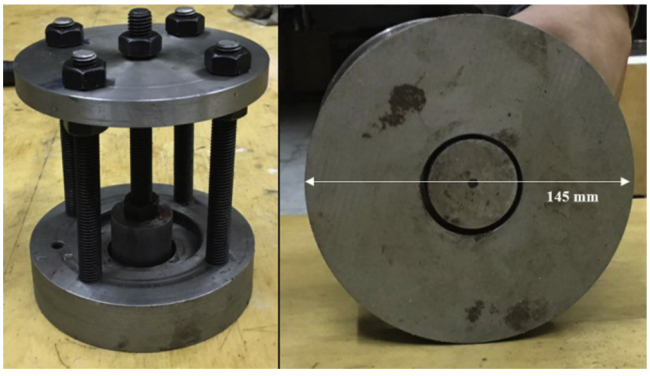

Fig. 4. Compaction tool for sample production inside and outside the internal sleeve.

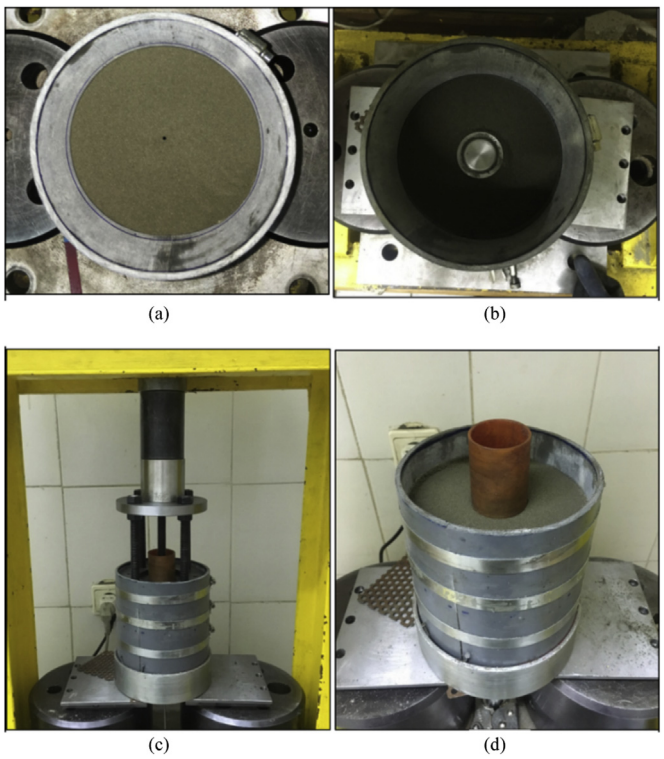

Fig. 5. Sample production: (a) Mixture of cement, sand and water after compaction till the sensor placement; (b) Embedment of the sensor with its hydraulic tube in the surrounding material; (c) Compaction of inclusion and surrounding material; and (d) Final view of synthetic sandstone sample in the cast.

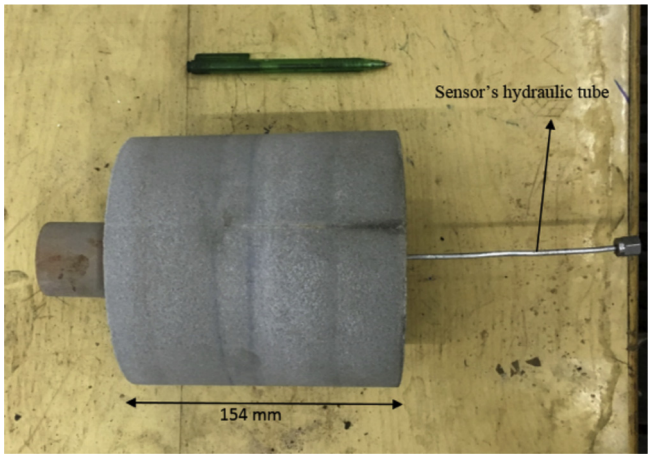

Fig. 6. Sample prepared for the main tests (note that the sample is compacted homogeneously and some lines on the sample are traces of marker from interior wall of cast).

oven at 80 °C for 24 h. Finally, it is taken out and cooled down for the main tests (Fig. 6). Note that the sample is compacted homogeneously and some lines on the exterior sample wall (as shown in Fig. 6) are traces of marker from interior cast wall.

2.2. Laboratory system

A schematic view of the laboratory setup is shown in Fig. 7. The main body of the system is a large-scale Hoek cell with a pressure capacity of 450 bar (1 bar = 0.1 MPa). The sample is placed in the cell, and the axial stress, confining stress and pore pressure are applied to the inclusion and the surrounding material. The main body of the system has five hydraulic outputs to measure and control the axial stress, confining stress, pore pressure, inclusion pressure and sensor pressure, respectively. These outputs are shown in Fig. 7 with gray boxes. They are electrically connected to a data acquisition system and a computer to monitor and record data continuously during tests (Fig. 8). Inclusion pressure increases and decreases at a constant rate using a screw pump during the tests simulating injection and depletion. The entire setup is shown in Fig. 9.

2.3. Sensor specifications and calibration test

To measure stress changes in laboratory tests, a small sensor is required. The sensor must be applicable in highly pressurized and stressed porous materials. For this, a hydraulic sensor with the diameter of 40 mm and 1 mm thick diaphragm is designed. The sensor is connected to a small hydraulic tube before being embedded in the sample. They are full of hydraulic oil during the tests. Pressure change is recorded by a pressure transducer connected at the end of the tube.

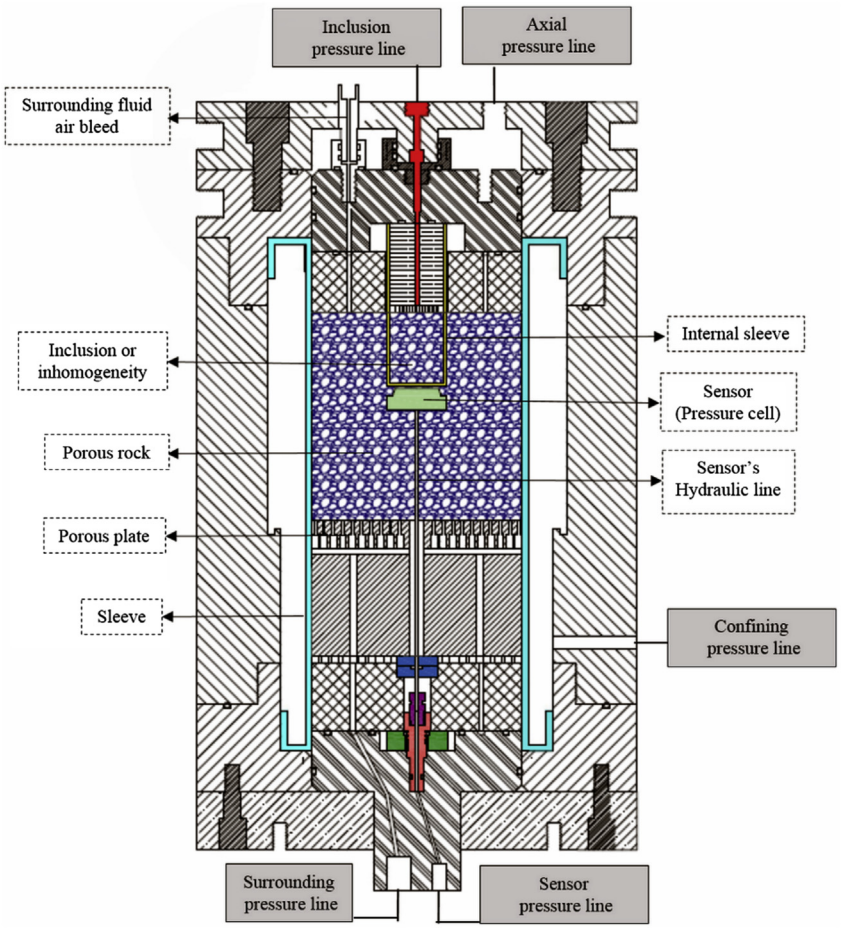

Fig. 7. Schematic view of main body for laboratory testing system.

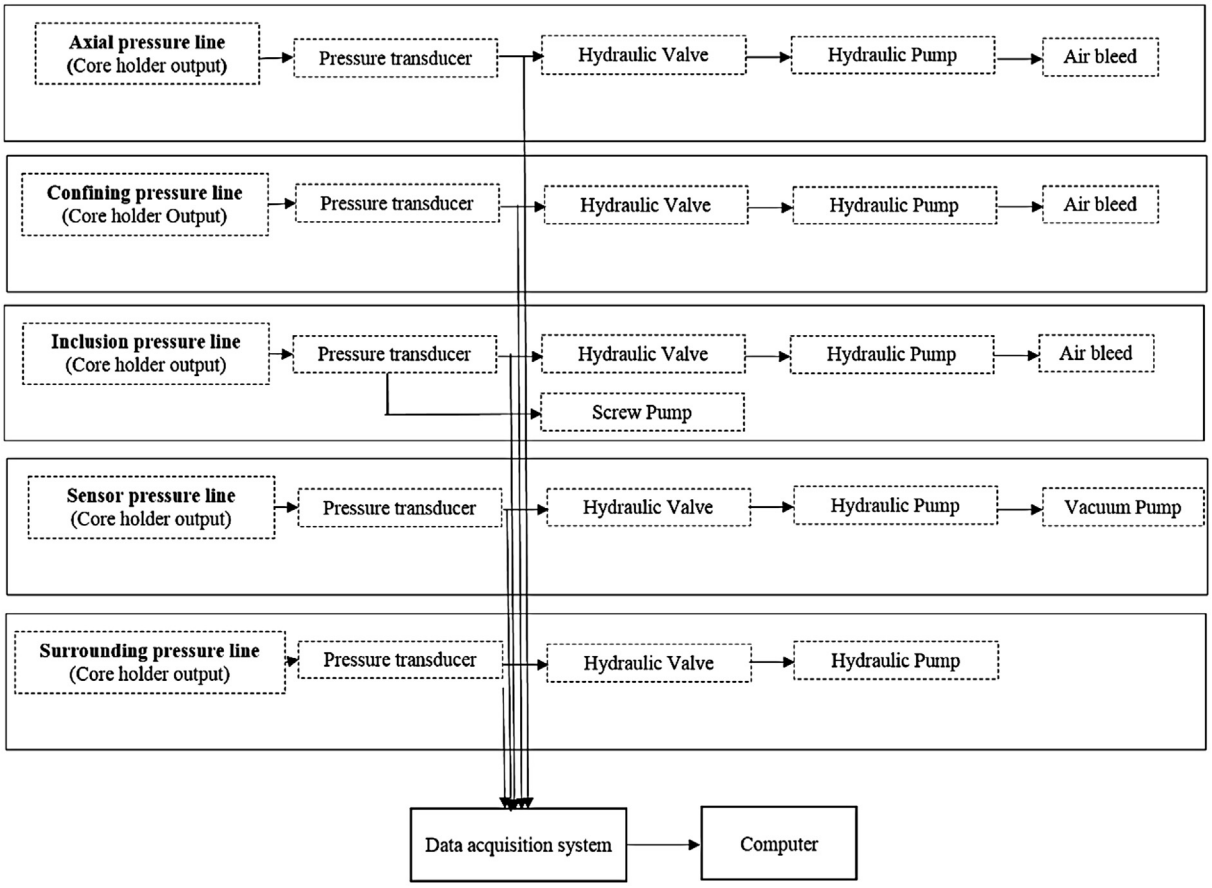

Fig. 8. Hydraulic and electrical circuits for five outputs of the main body of laboratory testing system.

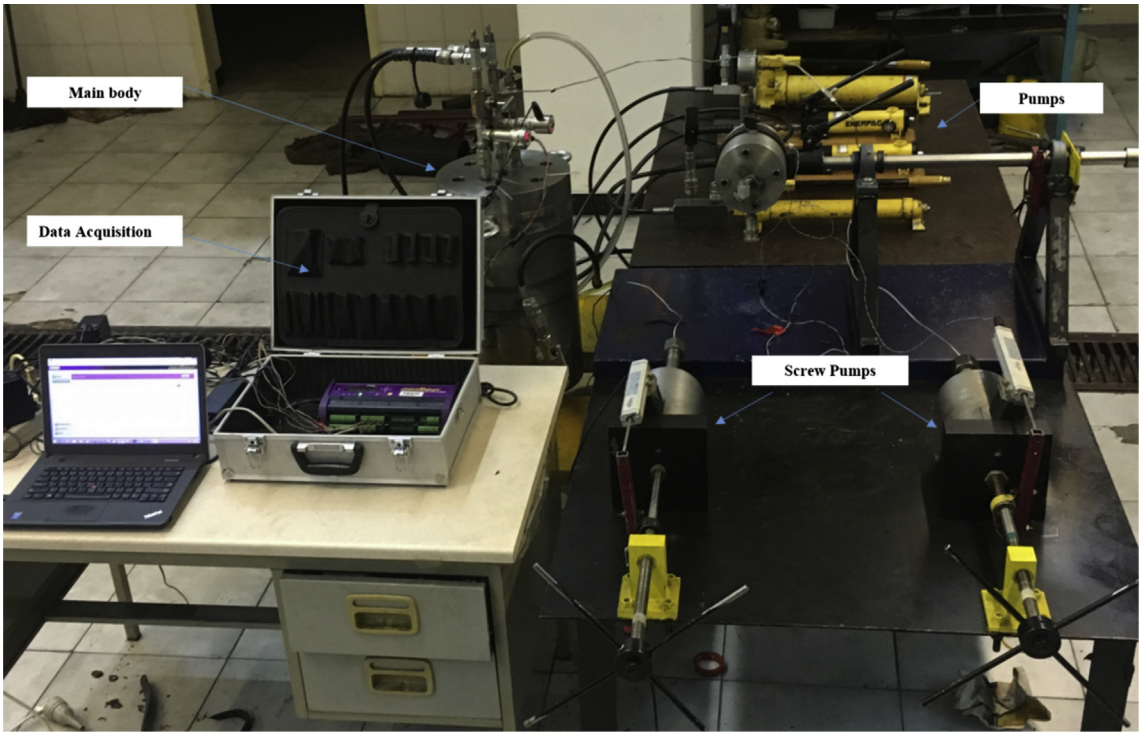

Fig. 9. Laboratory system and its accessories.

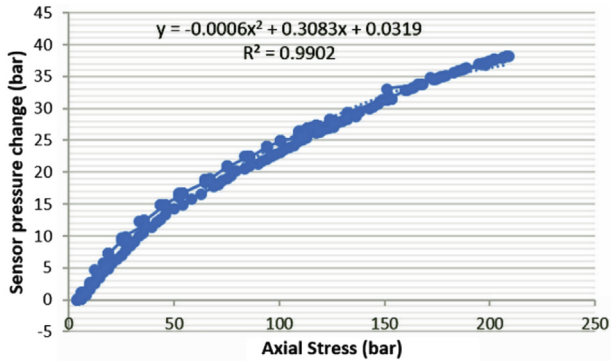

Fig. 10. Results of calibration test on the sensor.

Before performing the main tests, calibration test is carried out on a sensor embedded in a calibration synthetic sandstone sample to determine the sensor behavior. The sample is produced as per the procedures mentioned above, without internal sleeve and inclusion. Obviously, the mechanical properties of the calibration sample are identical to those of the surrounding material, as shown in Table 1. Results of calibration test are shown in Fig. 10, where the sensor pressure change is drawn versus the axial stress on the calibration sample. The pore pressure is kept constant at 1 bar during the test. According to Fig. 10, the sensor behavior is nonlinear. The results of calibration test are used to identify the magnitude of stress changes on the sensor's diaphragm during the main tests. Note that arching effect due to the presence of the sensor in the sample is ignored in calibration analysis for the main tests. The calibration test also shows that the sensor is not sensitive to loading speed and its response is reasonably repeatable. This is proved by applying loading and unloading conditions on the sensor at different rates.

After sample preparation, it is placed in a rubber sleeve with its accessories. Then the sensor and its tube are vacuumed to remove any captured air bubble and an initial setting pressure is applied (nearly 10 bar). The sample is placed in the Hoek cell and an initial hydrostatic stress is applied. After that, the inclusion and surrounding material are saturated with pore fluid, i.e. hydraulic oil in this project. All tests are conducted at four hydrostatic stress levels: 50 bar, 100 bar, 150 bar and 200 bar. At each level of hydrostatic stress, surrounding pore pressure is set, and then all valves are closed. Subsequently, using the screw pump, inclusion fluid pressure increases first and then decreases at a constant rate, simulating injection and depletion in a reservoir. Surrounding pressure is kept constant during injection or depletion of the inclusion. Changes in the sensor pressure are recorded by data acquisition system continuously during tests. Three tests are performed on three synthetic sandstone samples as mentioned previously, i.e. inclusion test, soft inhomogeneity and stiff inhomogeneity tests. After performing each test, the sample is taken out of the cell and cut by a cutting tool as shown in Fig. 11. This is to ensure that the sample has retained homogeneous elastic state after tests and the sensor is placed in its proper position.

2.4. Experimental results

Recorded data by the sensor are calibrated using the results of calibration test on the sensor (Fig. 10). According to the calibration test results, the sensor is stress-dependent. Since there is no information about the initial stress on the sensor, a value is assumed. This value is compared to that obtained by numerical models for simulating experimental tests.

Results from the inclusion test, soft inhomogeneity and stiff inhomogeneity tests are shown in Figs. 12–14, respectively. Stress

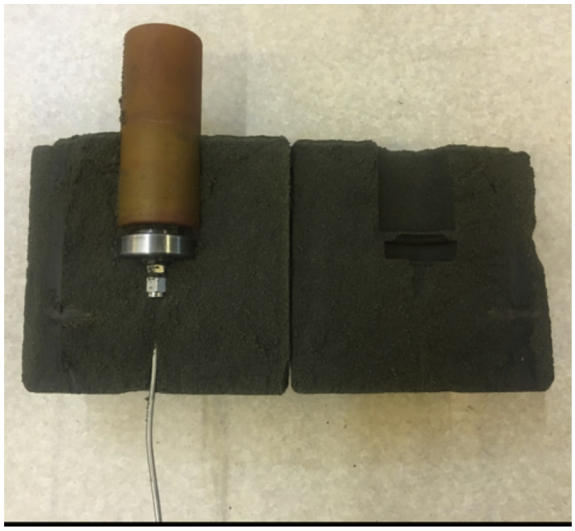

Fig. 11. The sample is cut after tests to ensure that there is no source of error.

changes recorded by the calibrated sensor are plotted versus the difference between the inclusion pressure and the surrounding pressure ($P_i - P_s$). Inclusion test results are shown in Fig. 12 at four hydrostatic stress levels: 50 bar, 100 bar, 150 bar and 200 bar. At each hydrostatic stress level, two or three tests are conducted at different surrounding pressures. The actual amount of hydrostatic confining stress (*C.S*) and surrounding pressure (*S.P*) are shown in the legend of figures. All tests start at nearly 1 bar of inclusion pressure. Therefore, the first and second routes represent injection and depletion, respectively. The results show that the injection and depletion curves are nearly the same at each test. The slope of the curves represents the surrounding vertical stress arching ratio, i.e. the coefficient of equations labeled on the curves in colored boxes. According to the results, some curves have a constant slope, while the other curves are nonlinear. For example, in Fig. 12a, the vertical stress change has nearly linear behavior, while in Fig. 12b–d, the curves tend to be nonlinear, especially at higher surrounding pressures. The reason is the nature of stress below the inclusion being either compressive or tensile. The initial vertical stress on the sensor may be of a tensile nature before injection starts due to primary loading and surrounding pore pressure in the sample. The presence of the soft internal sleeve also contributes to this effect. When the rock particle is in tensile mode, the sensor does not record data and only the surrounding pressure is applied on the sensor's diaphragm. On the other hand, when the sensor records data with a constant rate, it is in compressive loading mode induced by solid particles besides the surrounding fluid pressure. Obviously, at each hydrostatic confining stress level, tensile stress on the sensor is more likely to occur at higher surrounding pressures. During injection of the inclusion, the vertical stress on the sensor increases and changes from tensile to compressive. This causes a transitional part in the nonlinear curves when the vertical stress changes from tension to compression. Therefore, the obtained nonlinear curve has three parts: horizontal part representing the tensile stress (in the primary stage of injection), intermediate part representing stress transition (with the progress of injection), and linear part representing the compressive stress on the sensor (in the last stage of injection). These parts of curves are shown in Fig. 14c. Transitional response of the sensor, when the vertical stress changes from tensile to compressive, is produced because the sensor surface (the sensor's diaphragm) is gradually subjected to stress changes.

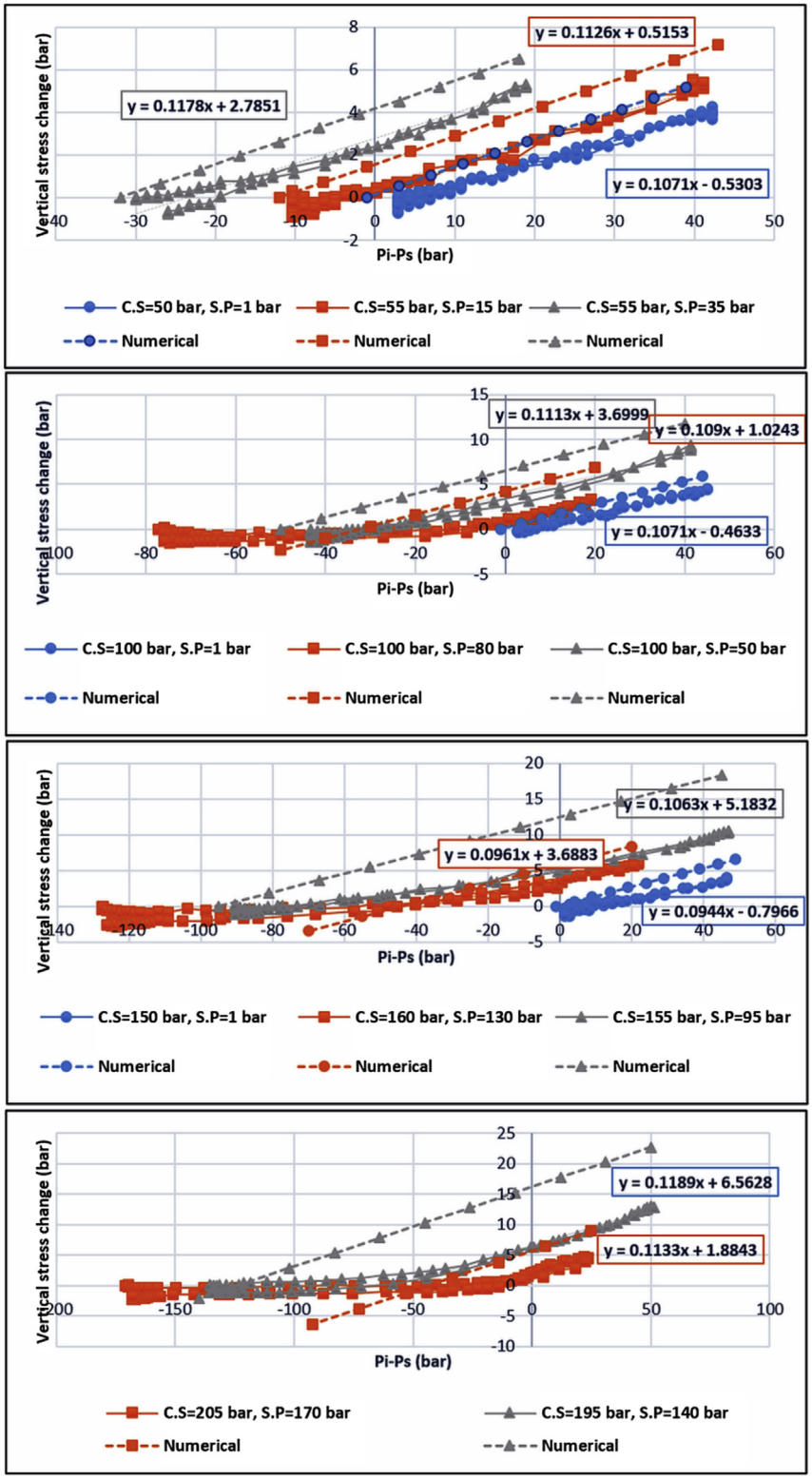

Fig. 12. Inclusion test results. Solid lines with markers are laboratory curves under different hydrostatic stresses. Stress arching ratio is the coefficient of each equation labeled beside the curve with the same color box. Dashed lines with markers are corresponding numerical results obtained from finite element models.

In other words, the sensor measures an average stress condition on its surface. For the nonlinear curves, the first and second parts are of no use for this research and only the value of stress arching ratio is obtained from the slope of the curves in the third part when the compressive stress acts on the sensor surface. According to Figs. 12–14, the slope (stress arching ratio) is nearly constant in the compressive part of the curves. It should be noted that the labeled equations on the curves correspond to the compressive parts. Dashed lines in the figures are related to numerical analysis, as discussed in the next section.

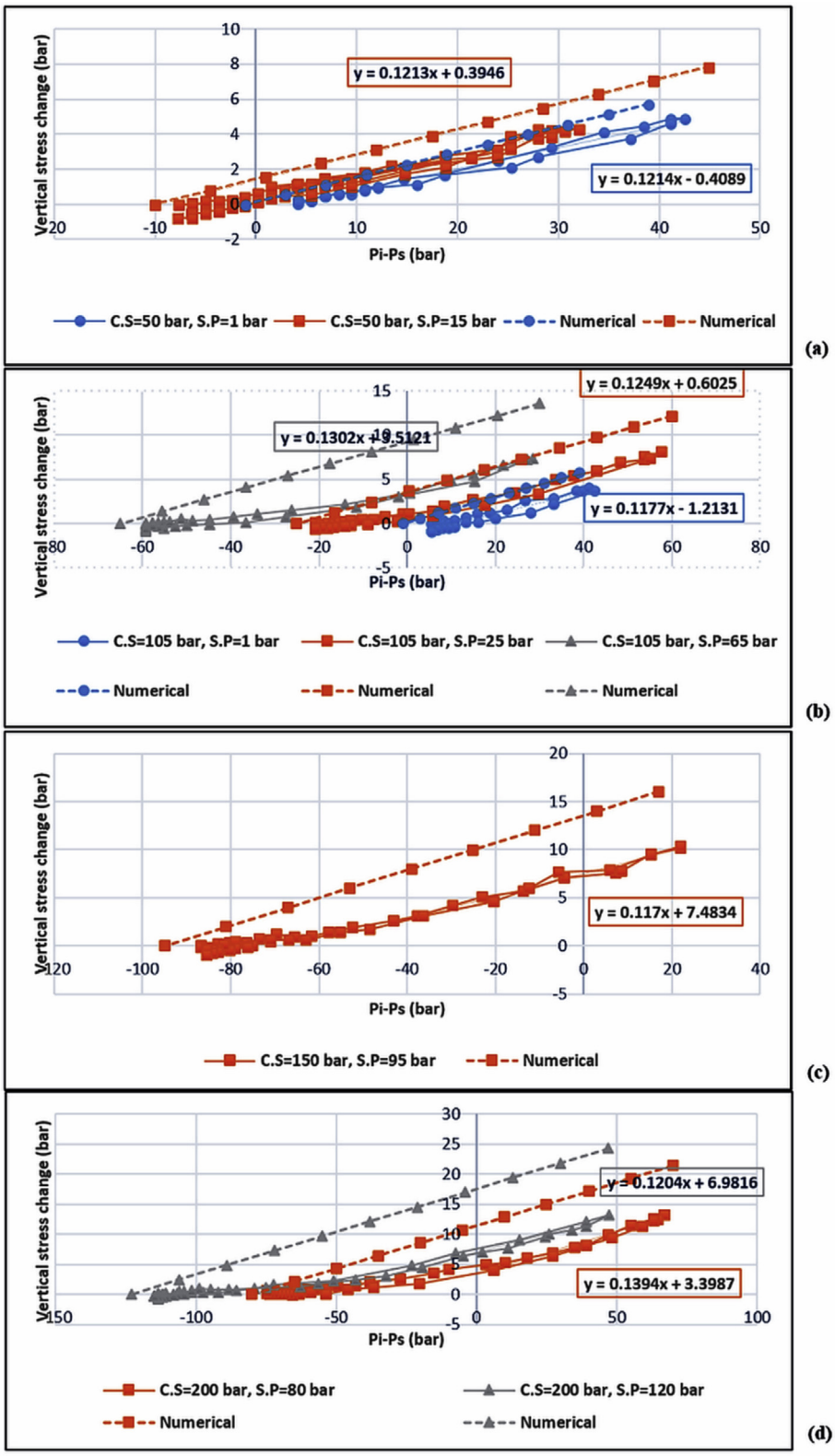

Fig. 13. Soft inhomogeneity test results. Solid lines with markers are laboratory curves under different hydrostatic stresses. Stress arching ratio is the coefficient of each equation labeled beside the curve with the same color box. Dashed lines with markers are corresponding numerical results obtained from finite element models.

According to Figs. 12–14, stress arching is nearly the same at any level of hydrostatic confining stress in each test. The values of vertical stress arching ratio are 0.11, 0.13 and 0.09 for inclusion test, soft and stiff inhomogeneity tests, respectively. These values are too small and close to each other. However, according to the literature, higher values of stress arching ratio with greater difference are expected. The reason is the existence of internal sleeve and the contrast of its mechanical property with that of

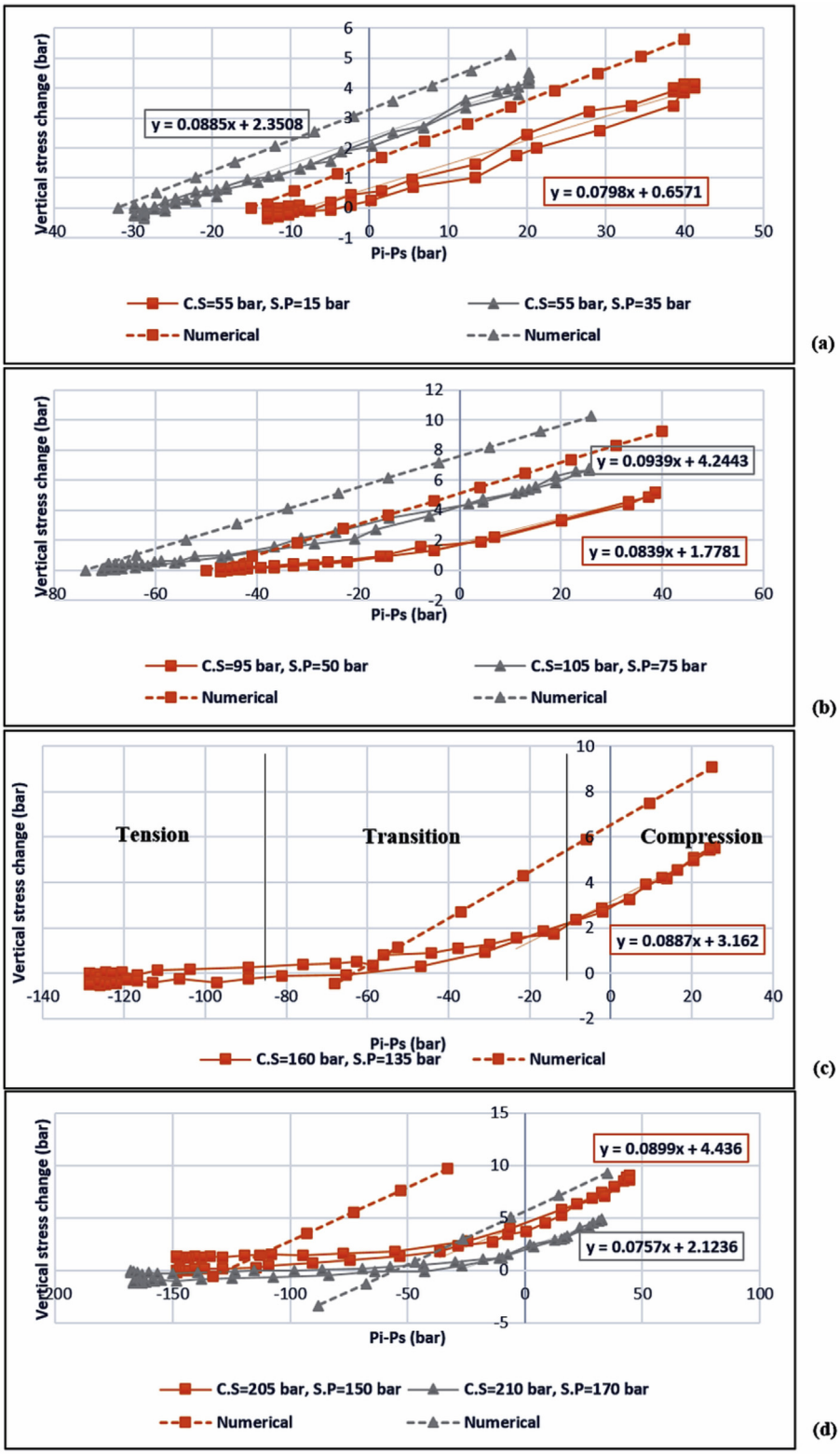

Fig. 14. Stiff inhomogeneity test results. Solid lines with markers are laboratory curves under different hydrostatic stresses. Stress arching ratio is the coefficient of the equation labeled beside each curve with the same color box. Dashed lines with markers are corresponding numerical experiment results obtained from finite element models.

the porous rock, as discussed in the following section, where the values of stress arching will be evaluated using numerical analysis of laboratory experiments and will be compared to the test results.

3. Numerical modeling of laboratory experiments

As mentioned in the previous section, analytical models cannot validate the test results because of their limitations for infinite

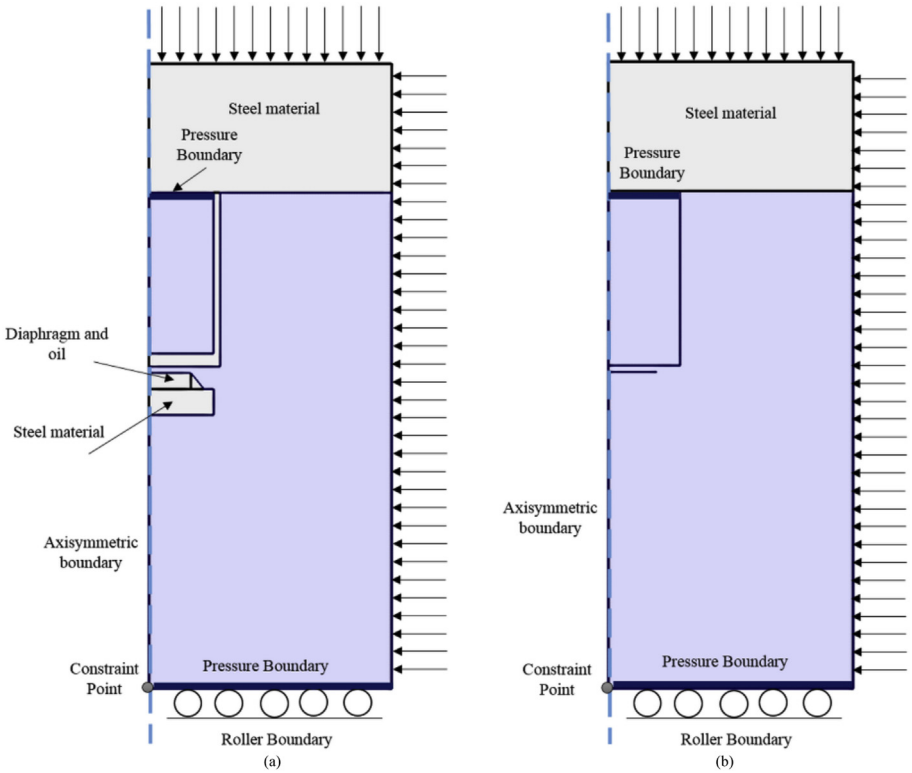

Fig. 15. Numerical models. Blue and gray domains have linear poroelastic and linear elastic model behaviors, respectively. (a) Numerical model for laboratory experiment with the same conditions as that in laboratory tests; and (b) Numerical model for sensitivity analysis of geomechanical parameters on stress arching ratio.

surrounding media. Therefore, the test results are checked by numerical models. A finite element poroelastic code is used for numerical modeling of laboratory experiments. The model geometry, domain behavior, and boundary conditions are shown in Fig. 15a. The model is axisymmetric and all test parts including steel spacer, internal sleeve, and the sensor are simulated. Blue and gray domains in the model have linear poroelastic and linear elastic behaviors, respectively. The thick blue line represents the pressure boundary of inclusion. Axial and confining loads are applied to the model in hydrostatic condition as the same as laboratory tests. Displacement and load boundary conditions are shown in the figure. All other boundaries (without pressure and load boundary conditions) have no-flow, free and continuity (variables across them are continuous) conditions. Mechanical properties for all parts of the model are shown in Tables 1 and 2. Uniaxial compression tests are carried out on cylindrical polyurethane samples which have the same properties as the internal sleeve to obtain the Young's modulus and Poisson's ratio (Table 2). The sensor diaphragm and hydraulic oil are simulated as an equivalent solid medium that has the mechanical properties of hydraulic oil. Normal stress on the sensor surface is obtained using average method. The model runs in a stationary mode in which time is excluded, thus fluid flow and mechanical equations are solved simultaneously. After primary stress and pore pressure are applied, injection and depletion are modeled through inclusion pressure boundary in a stepwise manner using step functions. Note that the actual stress on the sensor obtained from the numerical model is nearly compatible with the assumed value of stress for calibration analysis.

Numerical results obtained from the model shown in Fig. 15a are denoted with the dashed lines in Figs. 12–14 versus the laboratory results with the same color and marker. According to Figs. 12–14, the numerical results have constant slopes, almost the same as those of the laboratory data in the compressive parts. As mentioned in the previous section, some of the curves obtained from laboratory tests are not linear, especially at higher surrounding pressures, due to the existence of soft internal sleeve and the limitations of the sensor in recording tensile stresses. Therefore, there is a transitional part in the curves which represents the change of stress from tensile to compressive. These limitations cause incompatibility between laboratory results and numerical models in the nonlinear parts. While the valid values of the vertical stress arching ratio are the data recorded in the last stage of injection and they compare well with numerical results. In other words, the compatibility between laboratory and numerical results are proved by the comparison between the slope of the compressive parts (in the last stage of injection) and the constant slope obtained from numerical

Table 2
Mechanical properties of linear elastic parts (gray color) of model.

Model part	Young's modulus (MPa)	Poisson's ratio
Internal sleeve	22.2	0.3
Steel	200,000	0.4
Diaphragm and hydraulic oil	2000	0.45

Table 3
Stress arching ratio obtained from numerical models.

Tests	With sensor and internal sleeve	Without sensor and internal sleeve
Inclusion	0.13	0.23
Soft inhomogeneity	0.14	0.27
Stiff inhomogeneity	0.1	0.17

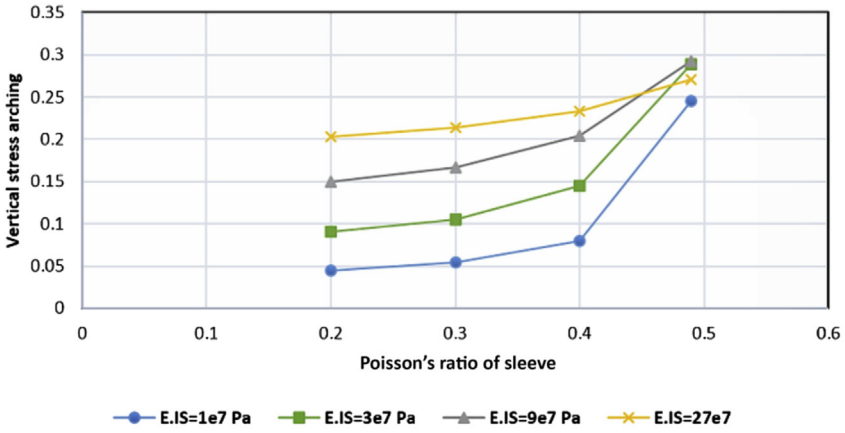

Fig. 16. Effect of internal sleeve's properties on stress arching for inclusion test.

models. It should be mentioned that in some of the tests that produce linear curves, numerical models fit reasonably well in all parts. Obviously, some errors are inevitable because of the nonlinear behavior of rock, limitations of the laboratory system and operator errors.

The stress arching ratios for the three tests at any hydrostatic confining stress level are shown in Table 3. According to the table, stress arching ratio values are nearly compatible with those obtained from laboratory experiment. As is mentioned in the previous section, higher values of stress arching ratio are expected. The numerical model without internal sleeve and sensor is established to understand their effects on the surrounding vertical stress arching. As shown in Fig. 15b, the model has the same conditions with the pervious one except that the former has no internal sleeve and sensor. The boundary conditions between the inclusion and the surrounding material are defined to be no-flow, free and continuous. Stress changes in the surrounding material are recorded on the line below the inclusion using the average method mentioned above. The results of stress arching ratio for the inclusion and inhomogeneity tests are also shown in Table 3.

Table 3 shows that the presence of internal sleeve and sensor has a significant effect on the values of stress arching ratio for three tests. Numerical analysis shows that the presence of sensor has a minor effect on the surrounding vertical stress arching; while the stress arching is affected by the mechanical properties of internal sleeve considerably. As shown in Fig. 16, the higher the Young's modulus (*E.IS*) and Poisson's ratio of internal sleeve are, the higher the vertical stress arching is. The presence of internal sleeve decreases the amount of stress arching and the effect of difference in the mechanical properties of inclusion and surrounding materials. This can be helpful in some reservoirs when intermediate layers have effects on the stress arching in the cap rock or adjacent formations. The mechanical properties of these layers reduce the effects of difference in the mechanical properties of reservoir and adjacent layers on the stress arching. This occurs in some complicated geological structures as is reported by Schutjens et al. (2012).

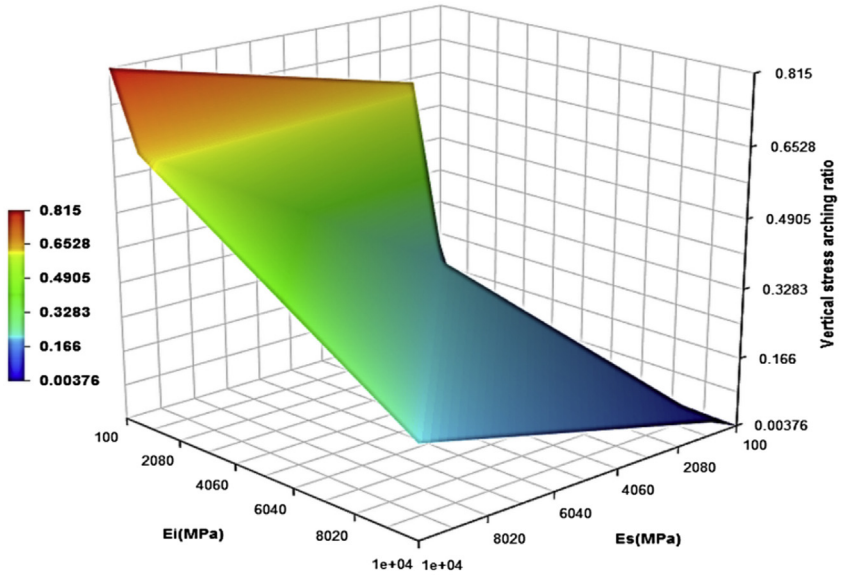

Fig. 17. Effects of Young's moduli on stress arching ratio. E_i is the Young's modulus of inclusion, and E_s is the Young's modulus of surrounding material. Poisson's ratio and Biot coefficient for both regions are identical (Poisson's ratio = 0.3, and Biot coefficient = 0.85).

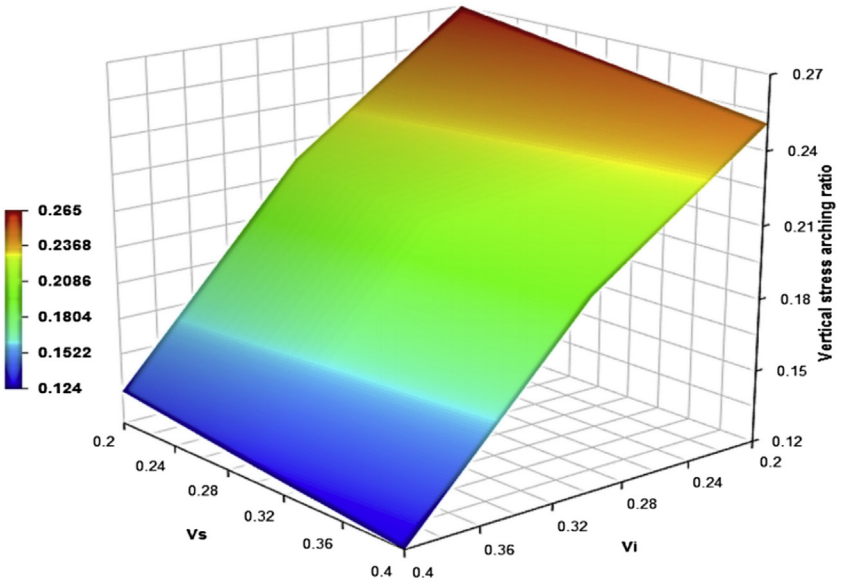

Fig. 18. Effects of Poisson's ratios on stress arching ratio. ν_i is the Poisson's ratio of inclusion, and ν_s is the Poisson's ratio of surrounding material. Young's modulus and Biot coefficient for both regions are identical (Young's modulus = 1 GPa, and Biot coefficient = 0.85).

4. Sensitivity analysis

Sensitivity analysis is conducted for the model without sensor and internal sleeve (Fig. 15b) to evaluate the influence of poroelastic properties on the surrounding vertical stress arching ratio. Results are shown in Figs. 17–19, where the surrounding vertical stress arching ratio is plotted versus the poroelastic properties of inclusion (inhomogeneity) and surrounding materials in three-dimensional (3D) graphs. Generally, as reported in the literature, the mechanical properties of inclusion have more effects on the stress arching than those of the surrounding materials. According to Fig. 17, the Young's modulus of inclusion (inhomogeneity) has more effect on the surrounding stress arching than that of the surrounding material, while the other properties (Poisson's ratio and Biot coefficient) are the same for the inclusion and surrounding material. This is valid for Poisson's ratio and Biot coefficient (Figs. 18 and 19). The Biot coefficient of surrounding material has almost no effect on the surrounding vertical stress arching. The Poisson's ratio of the surrounding material has minor effect than the inclusion (inhomogeneity) Poisson's ratio on the surrounding stress arching.

Eq. (5) can be checked by numerical model when the inclusion is placed at the center of the surrounding medium. Since the equation is valid for infinite surrounding media, stress arching ratio within the inclusion is plotted versus several scale factors of inclusion, as shown in Fig. 20. The horizontal stress arching ratio is the same because of symmetry. According to the figure, sum of the stress arching ratio is nearly equal to the analytical result at lower values of scale factor, thus it can be assumed that the surrounding medium

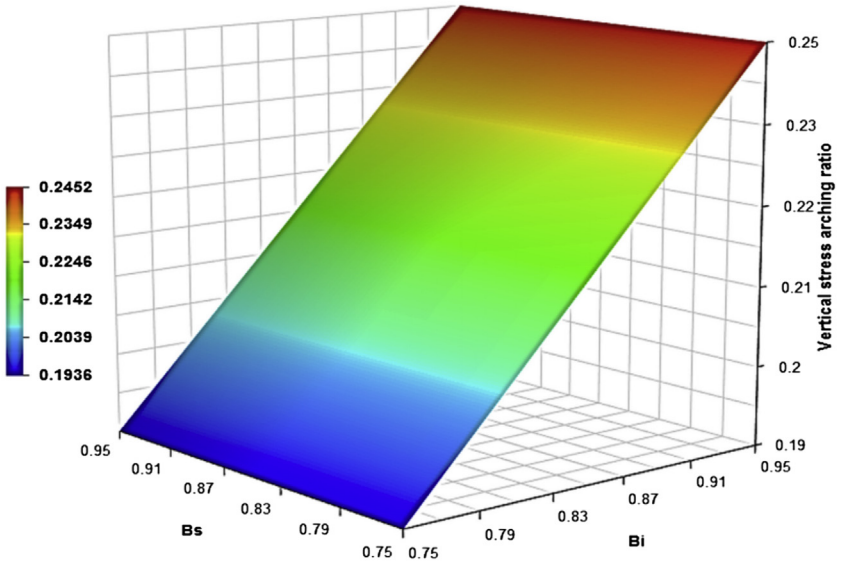

Fig. 19. Effects of Biot coefficients on stress arching ratio. B_i is the Biot coefficient of inclusion, and B_s is the Biot coefficient of surrounding material. Young's modulus and Poisson's ratio for both regions are identical (Young's modulus = 1 GPa, and Poisson's ratio = 0.3).

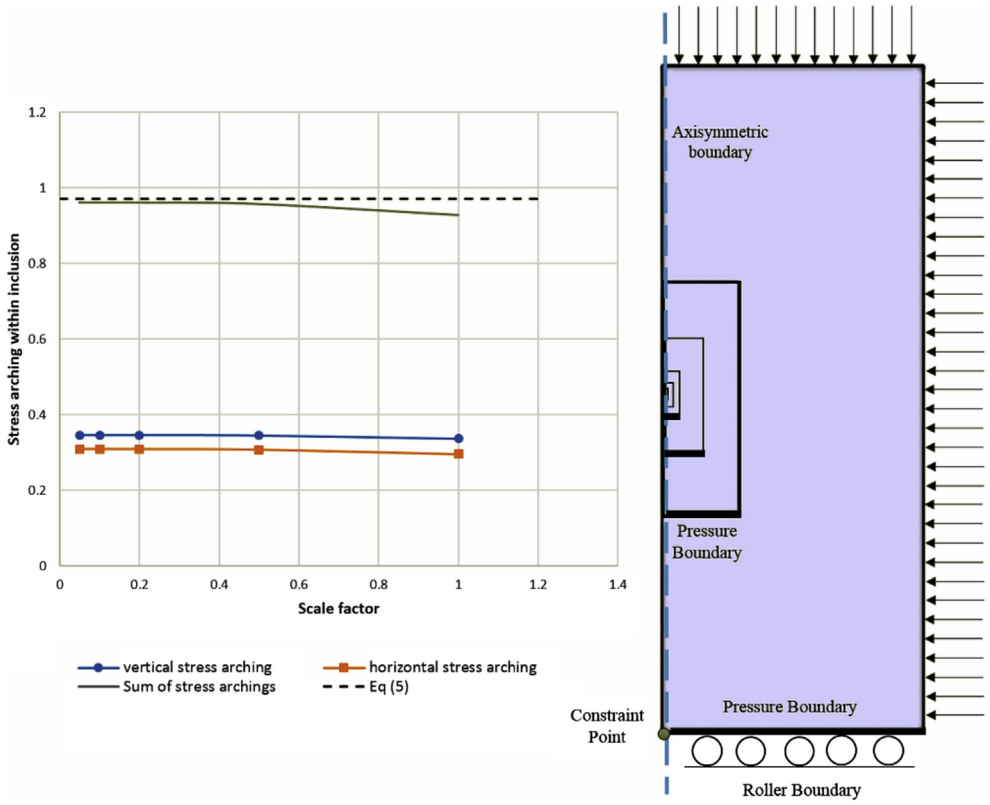

Fig. 20. Scale effect of inclusion on stress arching ratio within the inclusion and its validation by Eq. (5).

is infinite compared with the inclusion size. The Young's modulus, Poisson's ratio and Biot coefficient of the model are assumed as 1 GPa, 0.3 and 0.85, respectively.

5. Conclusions

Depletion or injection induced stress arching in porous rocks is a crucial parameter to estimate stresses and to understand the behavior of rocks in different conditions. In this paper, laboratory measurement of vertical stress arching in the surrounding rock is presented. A laboratory setup is designed for this purpose. Three tests (inclusion, soft inhomogeneity and stiff inhomogeneity tests) are conducted on large-scale synthetic sandstone samples. All tests are performed at different levels of hydrostatic stress and surrounding pressure. Injection and depletion are simulated using increasing and decreasing inclusion pressures while the confining stress and surrounding pressure are kept constant. Vertical stress change in the surrounding rock is recorded using a designed miniature sensor (pressure cell). Laboratory results show that in some tests, the vertical stress change in the surrounding medium is nonlinear, especially when the surrounding pressure is high. This is because of the presence of tensile stress on the sensor at the beginning of these tests. During injection, the stress on the sensor changes from tension to compression. This causes three parts in the laboratory curves: horizontal, intermediate and linear parts, representing the tensile stress, stress transition and compressive stress on the sensor, respectively. The slopes of the curves in the linear parts are the same for each test. This is known as the vertical stress arching ratio. Comparison of the stress arching ratios for three tests shows that they are small and close to each other, while it is expected to have higher stress arching ratio with greater difference among tests. This is caused by the internal sleeve and its mechanical property contrast with those of porous rock. Numerical analysis shows that the presence of internal sleeve can reduce the effects of mechanical property contrast between the inclusion (inhomogeneity) and the surrounding material in addition to the reduction in stress arching ratio values. This can be helpful in geomechanical analysis of reservoirs that are being surrounded by thin layers such as salt formations. Due to the limitations of analytical methods, test results are checked by numerical models. The results show a good compatibility with the test results. Sensitivity analysis using numerical models shows that the poroelastic properties of inclusion (inhomogeneity) have more effects on the surrounding stress arching than those of the surrounding part. Numerical models are validated by the analytical method using the assumption of infinite surrounding domain in the models. This is done as an indirect validation of laboratory tests.

Conflicts of interest

The authors wish to confirm that there are no known conflicts of interest associated with this publication and there has been no significant financial support for this work that could have influenced its outcome.

Acknowledgement

We are thankful to Mr. Behnam Rahimi Mohseni, MSc student in petroleum engineering, for his kind assistance in performing laboratory tests in Rock Mechanics Laboratory of the University of Tehran.

List of symbols

σ_v	Vertical total stress
σ_h	Minimum horizontal total stress

σ_H	Maximum horizontal total stress
σ'_v	Vertical effective stress
σ'_h	Minimum horizontal effective stress
P_p	Pore pressure
Δ	Differential operator
P_s	Surrounding pressure
P_i	Inclusion (inhomogeneity) pressure
γ_v	Vertical stress arching ratio
γ_h	Minimum horizontal stress arching ratio
γ_H	Maximum horizontal stress arching ratio
K	Deviatoric stress path
α	Biot coefficient
ν	Poisson's ratio
E	Young's modulus
$E.IS$	Young's modulus of internal sleeve
i	Subscript related to inclusion (inhomogeneity) material
s	Subscript related to surrounding material

References

Addis MA. The stress-depletion response of reservoirs. In: SPE annual technical conference and exhibition. Society of petroleum engineers (SPE); 1997. https://doi.org/10.2118/38720-MS.

Addis MA, Cauley MB, Kuyken C. Brent In-fill drilling programme: lost circulation associated with drilling depleted reservoirs. In: SPE/IADC drilling conference. SPE; 2001. https://doi.org/10.2118/67741-MS.

Aghighi MA, Rahman SS. Initiation of a secondary hydraulic fracture and its interaction with the primary fracture. International Journal of Rock Mechanics and Mining Sciences 2010;47(5):714–22.

Alassi HI, Li L, Holt R. Discrete element modeling of stress and strain evolution within and outside a depleting reservoir. Pure and Applied Geophysics 2006;163:1131–51.

Altmann JB, Müller BIR, Müller TM, Heidbach O, Tingay MRP, Weißhardt A. Pore pressure stress coupling in 3D and consequences for reservoir stress states and fault reactivation. Geothermics 2014;52:195–205.

Altmann JB, Müller TM, Müller BIR, Tingay MRP, Heidbach O. Poroelastic contribution to the reservoir stress path. International Journal of Rock Mechanics and Mining Sciences 2010;47(7):1104–13.

Asaei H, Moosavi M. Experimental measurement of compressibility coefficients of synthetic sandstone in hydrostatic conditions. Journal of Geophysics and Engineering 2013;10(5):55002. https://doi.org/10.1088/1742-2132/10/5/055002.

Biot MA. General theory of three-dimensional consolidation. Journal of Applied Physics 1941;12(2):155–64.

Eshelby JD. The elastic field outside an ellipsoidal inclusion. Proceedings of the Royal Society A: mathematical. Physical & Engineering Science 1959;252(1271):561–9.

Eshelby JD. The determination of the elastic field of an ellipsoidal inclusion, and related problems. Proceedings of the Royal Society A: Mathematical, Physical & Engineering Science 1957;241(1226):376–96.

Fjar E, Holt RM, Raaen AM, Risnes R, Horsrud P. Petroleum related rock mechanics, vol. 53. 2nd ed. Elsevier; 2008.

Gambolati G, Teatini P, Tomasi L. Stress–strain analysis in productive gas/oil reservoirs. International Journal for Numerical and Analytical Methods in Geomechanics 1999;23(13):1495–519.

Geertsma J. Land subsidence above compacting oil and gas reservoirs. Journal of Petroleum Technology 1973;25(6):734–44.

Goulty NR. Reservoir stress path during depletion of Norwegian chalk oilfields. Petroleum Geoscience 2003;9:233–41.

Hettema MH, Bostrom B, Pedersen ES. Depletion-induced stress changes in an HP/HT reservoir: calibration and verification of a full field geomechanical model. In: SPE annual technical conference and exhibition. SPE; 2009. https://doi.org/10.2118/124713-MS.

Hettema MH, Schutjens PMTM, Verboom BJM, Gussinklo HJ. Production-induced compaction of a sandstone reservoir: the strong influence of stress path. SPE Reservoir Evaluation & Engineering 2000;3(4):342–7.

Hillis RR. Pore pressure/stress coupling and its implications for rock failure. Geological Society 2003;216(1):359–68. London, Special Publications.

Holt RM, Flornes O, Li L, Fjær E. Consequences of depletion-induced stress changes on reservoir compection and recovery. In: Gulf rocks 2004, the 6th north America rock mechanics symposium (NARMS). American Rock Mechanics Association; 2004.

Holt RM, Gheibi S, Lavrov A. Where does the stress path lead? Irreversibility and hysteresis in reservoir geomechanics. In: The 50th U.S. Rock mechanics/geomechanics symposium. American Rock Mechanics Association; 2016.

Khan M, Teufel LW. The effect of geological and geomechanical parameters on reservoir stress path and its importance in studying permeability anisotropy. SPE Reservoir Evaluation & Engineering 2000;3(5):394–400.

Kim S, Hosseini SA. Study on the ratio of pore-pressure/stress changes during fluid injection and its implications for CO_2 geologic storage. Journal of Petroleum Science and Engineering 2017;149:138–50.

Li S, Sauer RA, Wang G. The Eshelby tensors in a finite spherical domain – Part I: theoretical formulations. Journal of Applied Mechanics 2006a;74(4):770–83.

Li S, Wang G, Sauer RA. The Eshelby tensors in a finite spherical domain – Part II: applications to homogenization. Journal of Applied Mechanics 2006b;74(4):784–97.

Lynch T, Fisher Q, Angus D, Lorinczi P. Investigating stress path hysteresis in a CO_2 injection scenario using coupled geomechanical-fluid flow modelling. Energy Procedia 2013;37:3833–41.

Mura T. Micromechanics of defects in solids. 2nd, revised edition. Kluwer Academic Publishers; 2013.

Orlic B. Some geomechanical aspects of geological CO_2 sequestration. KSCE Journal of Civil Engineering 2009;13(4):225–32.

Orlic B, Wassing BBT. A study of stress change and fault slip in producing gas reservoirs overlain by elastic and viscoelastic caprocks. Rock Mechanics and Rock Engineering 2013;46(3):421–35.

Rudnicki JW. Eshelby's technique for analyzing inhomogeneities in geomechanics. In: Leroy Y, Lehner F, editors. Mechanics of Crustal Rocks. CISM Courses and Lectures, vol. 533. Vienna, Austria: Springer; 2011. p. 43–72.

Rudnicki JW. Eshelby transformations, pore pressure and fluid mass changes, and subsidence. In: Auriault JL, Geindreau C, Royer P, Bloch JF, Boutin C, Lewandowska J, editors. Poromechanics II, proceedings of the 2nd Biot conference on poromechanics. Rotterdam: A.A. Balkema; 2002. p. 307–12.

Rudnicki JW. Alteration of regional stress by reservoirs and other inhomogeneities: stabilizing or destabilizing? In: Vouille G, Berest P, editors. Proceedings of the 9th ISRM international congress on rock mechancis. Rotterdam: A.A. Balkema; 1999. p. 1629–37.

Rudnicki JW. Fluid mass sources and point forces in linear elastic diffusive solids. Mechanics of Materials 1986;5(4):383–93.

Ruistuen H, Teufel LW, Rhett D. Influence of reservoir stress path on deformation and permeability of weakly cemented sandstone reservoirs. SPE Reservoir Evaluation & Engineering 1999;2(3):266–72.

Rutqvist J, Moridis GJ, Grover T, Silpngarmlert S, Collett TS, Holdich SA. Coupled multiphase fluid flow and wellbore stability analysis associated with gas production from oceanic hydrate-bearing sediments. Journal of Petroleum Science and Engineering 2012;92–93:65–81.

Sayers C, Schutjens P. An introduction to reservoir geomechanics. Leading Edge 2007;26:597–601.

Sayers CM. Sensitivity of time-lapse seismic to reservoir stress path. Geophysical Prospecting 2006;54(3):369–80.

Schutjens P, Hindriks K, Myers M. Depletion-induced reservoir compaction: two geomechanical models and their application in the planning of subsidence monitoring. American Rock Mechanics Association; 2008.

Schutjens PM, Kuvshinov B. On the wellbore stress change caused by drawdown and depletion: an analytical model for a vertical well in a thin reservoir. SPE Reservoir Evaluation & Engineering 2010;13(4):688–98.

Schutjens PMTM, Snippe JR, Mahani H, Turner J, Ita J, Mossop AP. Production-induced stress change in and above a reservoir pierced by two salt domes: a geomechanical model and its applications. SPE Journal 2012;17(1):80–97.

Segall P. Induced stresses due to fluid extraction from axisymmetric reservoirs. Pure and Applied Geophysics 1992;139(3–4):535–60.

Segall P. Stress and subsidence resulting from subsurface fluid withdrawal in the epicentral region of the 1983 Coalinga Earthquake. Journal of Geophysical Research: Solid Earth 1985;90(B8):6801–16.

Segall P, Fitzgerald SD. A note on induced stress changes in hydrocarbon and geothermal reservoirs. Tectonophysics 1998;289(1–3):117–28.

Segall P, Grasso JR, Mossop A. Poroelastic stressing and induced seismicity near the Lacq gas field, southwestern France. Journal of Geophysical Research: Solid Earth 1994;99(B8):15423–38.

Segura JM, Fisher QJ, Crook AJL, Dutko M, Yu JG, Skachkov S, Angus DA, Verdon JP, Kendall JM. Reservoir stress path characterization and its implications for fluid-flow production simulations. Petroleum Geoscience 2011;17(4):335–44.

Settari A. Reservoir compaction. Journal of Petroleum Technology 2002;54(8):62–9.

Soltanzadeh H, Hawkes CD. Induced poroelastic and thermoelastic stress changes within reservoirs during fluid injection and production. In: Acosta JL, Camacho AF, editors. Porous media: heat and mass transfer, transport and mechanics. New York: Nova Science Publishers, Inc.; 2009a. p. 27–56.

Soltanzadeh H, Hawkes CD. Assessing fault reactivation tendency within and surrounding porous reservoirs during fluid production or injection. International Journal of Rock Mechanics and Mining Sciences 2009b;46(1):1–7.

Soltanzadeh H, Hawkes CD. Semi-analytical models for stress change and fault reactivation induced by reservoir production and injection. Journal of Petroleum Science and Engineering 2008;60(2):71–85.

Soltanzadeh H, Hawkes CD. Predicting the stress changes induced by fluid production and injection in porous reservoirs. In: Proceedings of the 1st Canada-U.S. Rock mechanics symposium. American Rock Mechanics Association; 2007.

Soltanzadeh H, Hawkes CD, Sharma JS. Poroelastic model for production- and injection-induced stresses in reservoirs with elastic properties different from the surrounding rock. International Journal of Geomechanics 2007;7(5):353–61.

Terzaghi K. Erdbaumechanik auf Bodenphsikalischer Grundlage. F. Deuticke. 1925 (in German).

Teufel LW, Rhett DW, Farrell HE. Effect of reservoir depletion and pore pressure drawdown on in situ stress and deformation in the Ekofisk field, North Sea. In: Proceedings of the 32nd U.S. Symposium on rock mechanics (USRMS). A.A. Balkema; 1991.

Tingay MRP, Hillis RR, Morley CK, Swarbrick RE, Okpere EC. Pore pressure/stress coupling in Brunei Darussalam – implications for shale injection.

In: Van Rensbergen P, Hillis RR, Maltman AJ, Morley CK, editors. Subsurface sediment mobilization. Bath, UK: Geological Society of London; 2003. p. 369–79.

Wang F, Li X, Couples G, Shi J, Zhang J, Tepinhi Y, Wu L. Stress arching effect on stress sensitivity of permeability and gas well production in Sulige gas field. Journal of Petroleum Science and Engineering 2015;125:234–46.

Wright CA, Conant RA, Golich GM, Bondor PL, Murer AS, Dobie CA. Hydraulic fracture orientation and production/injection induced reservoir stress changes in diatomite waterfloods. In: SPE western regional meeting. Society of Petroleum Engineers; 1995. https://doi.org/10.2118/29625-MS.

Zoback M, Zinke J. Production-induced normal faulting in the Valhall and Ekofisk oil fields. In: Trifu C, editor. The Mechanism of induced seismicity. Birkhäuser Verlag; 2002. p. 403–20.

Dr. Hani Asaei is now working on Petroleum Geomechanics through experimental and numerical studies. He graduated from University of Tehran in February 2018. He designed two laboratory systems in his MSc and PhD theses: rock compressibility measurement system and rock poroelastic stress arching system. He was awarded as Talent student by the University of Tehran. He was university teacher for "Well Planning and Design" course for MSc students in Petroleum Faculty of Islamic Azad University (IAU). In addition, he taught as teacher assistant for BSc and MSc students for Rock Mechanics and Petroleum Geomechanics courses in the University of Tehran. He has worked as Rock Mechanics and Petroleum Geomechanics expert in some Iranian companies.

Dr. Mahdi Moosavi is Associate Professor in Rock Mechanics, presently working at the School of Mining Engineering at the University of Tehran, Iran. He obtained his PhD degree from Queen's University at Kingston, Ontario, Canada in 1997. He is presently the Head of Rock Mechanics Laboratory at the School of Mining Engineering and has vast experience in laboratory and field tests. His areas of expertise are geotechnical instrumentation, ground support systems and numerical modeling. He has published more than 120 papers in journals and conference proceedings and has been involved in many research projects. He is members of Iranian Society for Rock Mechanics (IRSRM), Iranian Geotechnical Society (IGS) and Iranian Society for Mining Engineering (ISME).

Dr. Mohammad Ali Aghighi holds his PhD degree in Petroleum Engineering from the University of New South Wales, Australia and MSc and BSc degrees in Mining Engineering from the University of Tehran, Iran. He was formerly an assistant professor at the University of Tehran, Iran. His areas of expertise are petroleum geomechanics, petroleum economics and numerical modeling of coupled phenomena in porous media and hydraulic fracturing. He has more than 20 years of experience in various academic institutions and industry. He has also published more than 40 papers in journals and conference proceedings.